

The Alcock-Paczyński test in redshifted twenty one centimeter maps

Adi Nusser

Physics Department and the Asher Space Research Institute, Technion, Haifa 32000, Israel

2 December 2024

ABSTRACT

We examine the possibility of constraining the cosmological mean mass and dark energy densities by an application of the Alcock-Paczyński test on redshifted 21-cm maps of the epoch of reionization. The 21-cm data will be provided as a function of frequency and angular positions on the sky. The ratio of the frequency to angular distance scales can be determined by inspecting the anisotropy pattern of the correlation function of brightness temperature. We assess the sensitivity of the distance ratio to the cosmological parameters and present a technique for disentangling geometrical distortions from redshift space distortions caused by peculiar motions.

Key words: cosmology: theory - intergalactic medium -large-scale structure of the universe

1 INTRODUCTION

Observations of the cosmic microwave background (CMB) and Type 1a Supernova place significant constraints on the physical parameters governing the evolution of the cosmological background (Spergel et al. 2003; Knop et al. 2003; Riess et al. 2004). The main parameters constrained by these observational data are the mean matter (mass) density, Ω_m , and the density of negative pressure energy (dark energy), Ω_v . Perhaps the most intriguing implication of the observations is the need for a dark energy component which dominates the energy budget in the Universe today (Ratra & Peebles 1988; Wetterich 1995; Coble, Dodelson & Frieman 1997; Turner & White 1997; Wang et al. 2000; Caldwell & Doran 2004; Kunz et al. 2004; Caresia, Matarrese & Moscardini 2004). By and large the constraints derived from these observations are sustained by other estimates based on analyses of cosmic flows (Strauss & Willick 1995; Nusser, Willick & Davis 1997; Zaroubi et al. 2001), abundance of rich galaxy clusters and its evolution (Bahcall et al. 2003; Ikebe et al. 2002; but see Vauclair et al. 2003) the mass-density power spectrum derived from galaxy redshift surveys (Percival et al. 2002; Zehavi et al. 2002; Tegmark et al. 2004), and the Ly- α forest (Croft et al. 2002, McDonald et al. 2000, Nusser & Haehnelt 2000, McDonald et al. 2004, Viel, Weller & Haehnelt 2004). Nevertheless all these constraints are derived from measurements at either very high (the CMB) or low and intermediate redshifts (SN and other data), excluding the wide redshift range the last scattering surface of CMB photons until $z \sim 4$. Here we present in detail a

technique for constraining the cosmological parameters by an application of the Alcock-Paczyński (AP) test (Alcock & Paczyński 1979; Hui, Stebbins & Burles 1999) on future data at $z \sim 10 - 30$. These data are maps of the redshifted 21-cm emission/absorption lines produced by H I in the high redshift universe (Field 1959; Sunyaev & Zel'dovich 1975; Hogan & Rees 1979; Subramanian & Padmanabhan 1993; Madau, Meiksin & Rees 1997). The 21-cm line is produced in the transition between the triplet and singlet sublevels of the hyperfine structure of the ground level of neutral hydrogen atoms. A patch of H I would be visible against CMB when its spin temperature T_s differs the CMB temperature, T_{CMB} . Various mechanisms exist for raising T_s significantly above T_{CMB} during the era of reionization. As a result a significant cosmological signal from the era of reionization should be expected (Field 1958 & 1959; Scott & Rees 1990; Madau, Meiksin & Rees 1997; Baltz, Gnedin & Silk 1998; Tozzi et al. 2000; Ciardi & Madau 2003; Chen & Miralda-Escude 2004; Gnedin & Shaver 2004; Nusser 2004; Ricotti, Ostriker & Gnedin 2004).

We advocate the application of the AP test on the correlations measured in three dimensional maps of 21-cm emission. These correlations are readily expressed in terms of angular separations and frequency intervals. In order to derive the correlations in terms of real space separations (measured for example in $h^{-1}\text{Mpc}$) one needs to know the mean density parameter, Ω_m , and the dark energy density Ω_v and its temporal evolution (or equivalently its equation of state). Constraints on these parameters can then be obtained by demanding isotropy of correlations in real space. There are

two main obstacles in implementing this program on future data. The first is foreground contamination (e.g. Oh & Mack 2003; Di Matteo, Ciardi & Muniati 2004) which we will not discuss here. The second is redshift distortions. The redshift coordinate of a patch of matter is given by the sum of its true real space coordinate and the its line of sight peculiar velocity (deviation from Hubble flow). The distribution of matter in redshift space should therefore be different from the real space distribution. According to the standard cosmological paradigm, the observed large scale structure have formed by gravitational amplification of tiny initial fluctuations (Peebles 1980, Peacock 1999). In late time linear theory the gravitational growth of mass density fluctuations is inevitable associated with coherent peculiar motions. Therefore, over large scales where linear theory is generally valid the density in redshift space appears more clustered than in real space. Further, because because redshift and real space coordinates differ only in the line of sight direction, the structure in redshift space would appear anisotropic. On small scales random motions are important, causing a suppression of clustering in redshift space. Here we restrict the analysis to linear theory which is valid at the high redshifts ($z \sim 10 - 30$) and the physical scales ($\gtrsim 1 \text{ h}^{-1} \text{Mpc}$) we consider. Redshift distortions, in the linear as well the non-linear regime, have been investigated in great detail in relation to the galaxy redshift surveys (Peebles 1980; Davis & Peebles 1983; Kaiser 1987; Hamilton 1992; Cole, Fisher & Weinberg 1994; Nusser & Davis 1994, Fisher & Nusser 1996; Taylor & Hamilton 1996; Zaroubi & Hoffman 1996; Hatton & Cole 1998; Desjacques et al. 2004) and to a lesser extent in relation to 21-cm maps (Illiev et al. 2002; Furlanetto, Sokasian & Hernquist 2004; Barkana & Loeb 2004).

In this paper we show that the pattern of redshift space anisotropies is quite distinct from the geometrical distortions introduced by an erroneous choice of the cosmological parameters. Further, we show that an application of the AP test will provide useful constraints on the cosmological parameters if the correlation function of the cosmological 21-cm brightness temperature could be estimated to within a 20% accuracy.

The outline of the paper is as follows. In §2 the relation between 21-cm emission/absorption and the gas density is briefly summarized. §3 describes in some detail redshift distortions in the linear regime and the expected anisotropy the density correlation function in redshift space. In §4 the dependence of geometrical distortions on the cosmological parameters is explored. §5 shows how to distinguish between geometrical and redshift space distortions. We conclude with a short discussion in §6.

2 THE BRIGHTNESS TEMPERATURE

Intensities, $I(\nu)$, at radio frequency are expressed in terms of brightness temperature defined as $T_b = I(\nu)c^2/2k\nu^2$, where c is the speed of light and k is Boltzman's constant (Wild 1952). The *differential brightness temperature* (hereafter, DBT) against the CMB of a small patch of gas with spin temperature T_s at redshift z is (e.g. Ciardi & Madau

2003),

$$\begin{aligned} \delta T_b &= 16 \text{ mK} x_{\text{HI}}(1 + \delta) \left(1 - \frac{T_{\text{CMB}}}{T_s} \right) \\ &\times \left(\frac{\Omega_b h}{0.02} \right) \left[\left(\frac{1+z}{10} \right) \left(\frac{0.3}{\Omega_m} \right) \right]. \end{aligned} \quad (1)$$

where x_{HI} are is the fraction of H I in the patch. The quantity $\delta = \rho/\bar{\rho} - 1$ is the density contrast of the gas. The fraction x_{HI} may depend on position, \mathbf{r} , and the density contrast, δ (e.g. Knox et al. 1998, Buscoli et al. 2000, benson et al. 2001). This dependence is mainly dictated by the nature of the ionizing radiation and the spatial distribution of its sources. If the early staged of reionization are dominated by X-ray photons which have very large mean free path then x_{HI} at any point in space is determined by the equilibrium between photoionization and recombinations (e.g. Ricotti & Ostriker 2004). In contrast, UV photons from stellar sources have a short mean free path. Therefore, in the presence of UV photons alone reionization proceeds in a patchy way with x_{HI} very close to zero in ionized regions and unity otherwise. We model reionization in the presence of X-rays and UV photons as follows. We assume that the explicit dependence of x_{HI} on δ outside the regions ionized by UV is linear so that (Barkana & Loeb 2004),

$$x_{\text{HI}}(\mathbf{r}, \delta) \propto \mathcal{M}(\mathbf{r}) \left[1 + \frac{\partial \ln x_{\text{HI}}}{\partial \delta} \delta \right], \quad (2)$$

where $\mathcal{M}(\mathbf{r})$ is termed the mask and is either zero or unity. The expansion of x_{HI} to first order in δ is justified here since we only consider correlations on large scales.

3 REDSHIFT DISTORTIONS

For simplicity of discussion we consider a region in the shape of a cubic box at redshift z . Further, we assume the “distant observer limit” (e.g. Kaiser 1987, Zaroubi & Hoffman 1996) according to which the box is small compared to its distance from the observer. We work with a Cartesian coordinate system defined by the axes of the box assuming that one of these axes is in the direction of the line of sight to the box. The box is assumed to be comoving with the Hubble flow and large enough so that the center of mass of matter inside it is also comoving with the Hubble flow.

In the coordinate system attached to the box, let \mathbf{v} and \mathbf{r} be, respectively, the physical peculiar velocity (deviations from Hubble flow) and physical real space coordinate (i.e. Eulerian) of a particle, both expressed in km s^{-1} . The redshift space coordinate is defined as $\mathbf{s} = \mathbf{r} + v_{\parallel} \hat{\mathbf{l}}$, where $\hat{\mathbf{l}}$ is a unit vector in the line of sight direction and $v_{\parallel} = (\hat{\mathbf{l}} \cdot \mathbf{v})$ is the line of sight peculiar velocity^{*}. It convenient to denote the components of \mathbf{r} parallel and perpendicular to the line of sight by r_{\parallel} and \mathbf{r}_{\perp} , respectively. Using similar notation for \mathbf{s} we find $\mathbf{s}_{\perp} = \mathbf{r}_{\perp}$ and $s_{\parallel} = r_{\parallel} + v_{\parallel}$.

^{*} The observed redshift coordinate also contains contributions from the cosmological expansion and from the peculiar motion of the observer. However, these contributions do not amount to any systematic effect.

Only in the absence of peculiar motions (both thermal and cosmological) the density contrast, δ , appearing in (1) refers to the actual real space density contrast, δ^r . In the presence of peculiar motions δ is equal to the gas density in redshift space, δ^s . This is given by

$$1 + \delta^s(s_\perp, s_\parallel) = \int dr_\parallel [1 + \delta^r(\mathbf{r}_\perp, r_\parallel)] G[r_\parallel + U(\mathbf{r}_\perp, r_\parallel) - s_\parallel], \quad (3)$$

where we have decomposed the line of sight peculiar velocity into a smooth component $U(\mathbf{r})$ and a random thermal component, v_{th} having a gaussian probability distribution function, $G(v_{\text{th}})$, of mean zero and rms σ_{th} . In the following we assume that σ_{th} is negligible so that G reduces to a Dirac delta function. In this case we obtain

$$1 + \delta^s(\mathbf{s}) = [1 + \delta^r(\mathbf{r})] \left(1 - \frac{dr_\parallel}{ds_\parallel} \right), \quad (4)$$

where r_\parallel is determined by $r_\parallel + U(\mathbf{r}_\perp, r_\parallel) = s_\parallel$. Expanding (4) to first order in δ and U yields

$$\delta^s(\mathbf{r}) = \delta^r(\mathbf{r}) - \frac{dU}{dr_\parallel}. \quad (5)$$

Note that to first order this last relation could equally be expressed as a function of \mathbf{s} rather than \mathbf{r} (Nusser & Davis 1994). The term dU/dr_\parallel introduces anisotropies in the density field in redshift space. Supplemented with a relation between the velocity and density fields of the gas, the relation (5) allows us to determine δ^s from δ^r . On large scale, a density-velocity relation between the real space mass density and velocity fields can be obtained using linear perturbation theory (e.g. Peebles 1980; Peacock 1999). This relation reads

$$\delta^r = -\Omega_m^{-0.6} \nabla \cdot \mathbf{v}. \quad (6)$$

As an illustration of redshift distortions we show in figure (2) slices of the density fields in real and redshift spaces in the bottom left and top left columns, respectively. The real space density field is a gaussian random field generated with the linear density power spectrum of the cold dark matter cosmology (CDM) with $\Omega_m = 0.3$. The linear relations (5) and (6) have been used to derive δ^s for a line of sight in the y -direction. The density fields are shown in a slice of $128 \text{ h}^{-1} \text{Mpc}$ on the side. To improve the visual presentations the fields have been smoothed with a gaussian window of $3 \text{ h}^{-1} \text{Mpc}$ width. The normalization is arbitrary and the contour spacing is 2. A comparison between the top left and bottom left panels reveals significant differences between δ^s and δ^r . The lack of isotropy in the contour maps of δ^s is also clear (see Kaiser 1987 for more details).

The relation (6) can easily be generalized to account for any *bias* between δ^r and the actual mass density, δ_m^r . To first order in the density contrast such a bias can be described by $\delta^r = b\delta_m^r$ where b is a constant. Then the relation (6) is modified by multiplying the right hand side by b . Hamilton (1992) used the linear relations (5) and (6) in order to express the redshift space density correlation function $\xi^s = \langle \delta^s(\mathbf{r}_0) \delta^s(\mathbf{r}_0 + \mathbf{r}) \rangle_{\mathbf{r}_0}$ in terms of the real space correlation $\xi^r = \langle \delta^r(\mathbf{r}_0) \delta^r(\mathbf{r}_0 + \mathbf{r}) \rangle_{\mathbf{r}_0}$ as follows,

$$\xi^s(r_\parallel, \mathbf{r}_\perp) = \xi_0(r) P_0(\mu) + \xi_2(r) P_2(\mu) + \xi_4(r) P_4(\mu), \quad (7)$$

where r_\parallel and \mathbf{r}_\perp are the components of \mathbf{r} parallel and perpendicular to the line of sight, $\mu = r_\parallel/r$ is cosine the angle between \mathbf{r} and the line of sight, and P_l is the l^{th} order Legendre polynomial: $P_0 = 1$, $P_2 = (3\mu^2 - 1)/2$, $P_4 = (35\mu^4 - 30\mu^2 + 3)/8$, and $P_6 = (231\mu^6 - 316\mu^4 + 105\mu^2 - 5)/16$ (we list P_6 for subsequent use). Further,

$$\xi_0(r) = \left(1 + \frac{2}{3} + \frac{1}{5}\beta^2 \right) \xi^r(r) \quad (8)$$

$$\xi_2(r) = \left(\frac{4}{3}\beta + \frac{4}{7}\beta^3 \right) [\xi^r(r) - \bar{\xi}^r] \quad (9)$$

$$\xi_4(r) = \frac{8}{35}\beta^2 \left[\xi^r(r) + \frac{5}{2}\bar{\xi}^r - \frac{7}{2}\bar{\bar{\xi}}^r \right] \quad (10)$$

where $\beta = \Omega_m^{0.6}/b$, $\bar{\xi}^r = 3r^{-3} \int_0^r \xi^r(s) s^2 ds$, and $\bar{\bar{\xi}}^r = 5r^{-5} \int_0^r \xi^r(s) s^4 ds$.

4 GEOMETRICAL DISTORTIONS

Twenty one centimeter maps will be readily provided in terms of the frequency along the line of sight direction and angular positions on the sky in the perpendicular plane. An observed frequency interval $\Delta\nu$ corresponds to a physical separation (in km s^{-1}), Δr_\parallel , of

$$\Delta r_\parallel = \frac{\Delta\nu}{1420 \text{ Hz}} \frac{c}{1+z}. \quad (11)$$

This relation is independent of the cosmological parameters. The projected separation (also in km s^{-1}), $\Delta\mathbf{r}_\perp$, corresponding to an angular separation of $\Delta\theta$ is

$$\Delta\mathbf{r}_\perp = \Delta\theta H D_A(z), \quad (12)$$

where $D_A = D_A(\Omega_m, \Omega_v, z)$ is the angular diameter distance and $H(\Omega_m, \Omega_v, z)$ is the Hubble function evaluated at redshift z . Therefore, for a given angular separation one needs to know the cosmological parameters in order to determine $\Delta\mathbf{r}_\perp$. The dependence $H D_A$ on the cosmological parameters is illustrated in figure (1) which shows the quantity $1/(H D_A)$ for cosmological models with and without a dark energy component (Lima & Alcaniz 2000). We assume a dark energy equation of state of the form $P_v = w\rho_v$, where P_v and ρ_v are, respectively, the pressure and density of the dark energy component, and w is constant. This equation of state implies $\rho_v \propto (1+z)^{3(1+w)}$ and so $w = -1$ describes a cosmological constant (constant ρ_v). We do not consider here $w < -1$. The figure shows $1/(H D_A)$ normalized to its value[†] for $\Omega_m = 0.3$, $\Omega_v = 0.7$ and $w = -1$. The solid line in the figure is for an open universe with $\Omega_v = 0$. All remaining curves are for a flat universe ($\Omega_m + \Omega_v = 1$) and they correspond to several values of w as indicated in the figure. The distance ratio is clearly sensitive to the assumed cosmological parameters. For the models plotted in the figure the maximal difference is about 40% at $\Omega_m = 0.2$. The panels to the right of figure (2) illustrate the nature of the geometrical distortions. The top (bottom) panel show the

[†] In this paper the numerical values of Ω_m and Ω_v always correspond to $z = 0$.

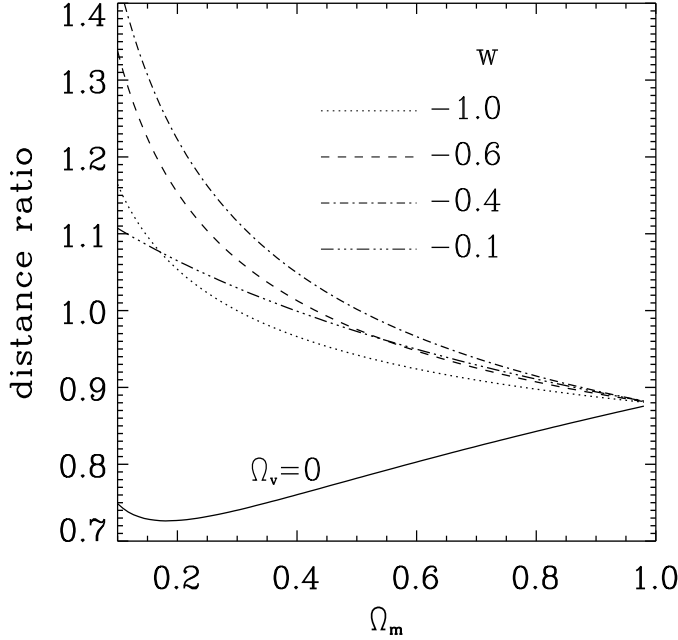


Figure 1. The dependence of the distance ratio $1/(HDA)$ at $z = 20$ on the assumed cosmological parameters. The ratio is normalized to its value at $\Omega_m = 0.3$, $\Omega_v = 0.7$, and $w = -1$. The solid curve is for an open universe with matter content only. All other curves correspond to universes with $\Omega_m + \Omega_v = 1$ for various values of w , as indicated in the figure.

density contours obtained by stretching the vertical (horizontal) axis of the slice in the left bottom panel 25%. The distinction between geometrical and redshift space distortions is readily seen by comparing these maps the density field in redshift space shown in the left top panel. Redshift distortions amplify the density fluctuations, while geometrical distortions merely stretch the contours.

In the absence of peculiar motions and foreground contamination the correlation function of the brightness temperature is isotropic for the true Ω_m , Ω_v , and w . However, we expect redshift distortions to be present as density fluctuations are associated with peculiar motions under the action of gravity. We show in the next section how to disentangle the geometrical from redshift distortions, allowing an estimation of the cosmological parameters from the isotropy pattern of the correlation function.

In the remainder of this section we derive several relations for later use. The relation between redshift and real space correlations is invariant under an isotropic scaling transformation of the form $\mathbf{r} \rightarrow g\mathbf{r}$, where g is a constant. Therefore, without loss of generality the effect of an incorrect choice of the cosmological parameters can be described by a transformation of the type $\tilde{r}_\parallel = r_\parallel/(1+\alpha)$ and $\tilde{\mathbf{r}}_\perp = \mathbf{r}_\perp$, where $(1+\alpha)$ is the ratio of the true value of HDA to the assumed value. For clarity of notation, we place a tilde over functions defined in the space of \tilde{r}_\parallel and $\tilde{\mathbf{r}}_\perp$. If $f = f(r_\parallel, \mathbf{r}_\perp)$ then

$$\tilde{f}(\tilde{r}_\parallel, \tilde{\mathbf{r}}_\perp) \equiv f[(r_\parallel, \mathbf{r}_\perp)], \quad (13)$$

We can easily verify that the correlation function of d com-

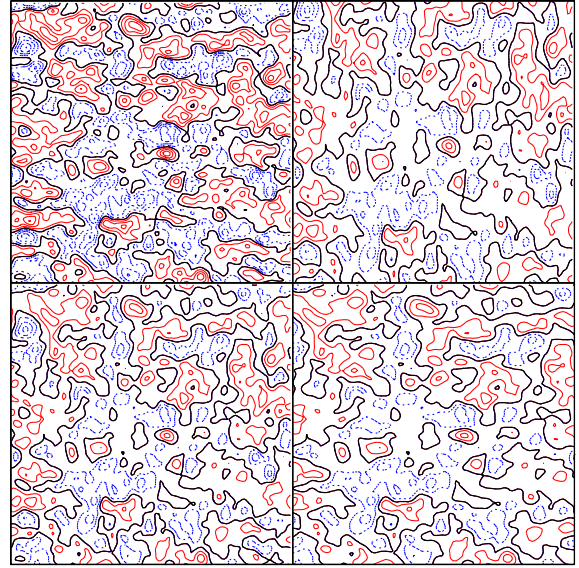


Figure 2. An illustration of the redshift and geometrical distortions. The bottom left panel with the isotropic contours shows the density field in real space. The top left is the corresponding redshift space density field obtained from the linear relations (5) and (6) for a line of sight along the vertical axis. The top right and the bottom right panels illustrate geometrical distortions parallel and perpendicular the line of sight, respectively. These distortions are for a 25% difference between the assumed and true distances.

puted in the space of $(\tilde{r}_\parallel, \tilde{\mathbf{r}}_\perp)$ is

$$\tilde{\xi}^s(\tilde{r}_\parallel, \tilde{\mathbf{r}}_\perp) = \xi^s[(1+\alpha)\tilde{r}_\parallel, \tilde{\mathbf{r}}_\perp]. \quad (14)$$

According to (13), if $f = f(r)$ is independent of the direction of \mathbf{r} , then

$$\tilde{f}(\tilde{r}_\parallel, \tilde{\mathbf{r}}_\perp) = f(r) \quad (15)$$

where $r = \sqrt{(1+\alpha)^2\tilde{r}_\parallel^2 + \tilde{\mathbf{r}}_\perp^2} = \tilde{r}\sqrt{(1-\alpha)^2\tilde{\mu}^2 + (1-\tilde{\mu}^2)}$. To first order in α we find

$$\tilde{f}(\tilde{r}_\parallel, \tilde{\mathbf{r}}_\perp) = f(\tilde{r}) \left[1 + \alpha\tilde{\mu}^2 \frac{d \ln f(\tilde{r})}{d \ln \tilde{r}} \right]. \quad (16)$$

We will also need the first order (in α) relation

$$\mu^2 = \tilde{\mu}^2 + 2\alpha\tilde{\mu}^2(1-\tilde{\mu}^2). \quad (17)$$

between $\tilde{\mu} = \tilde{r}_\parallel/\tilde{r}$ and $\mu = r_\parallel/r$.

5 DISTORTIONS IN TWENTY ONE CM MAPS

We assume that $T_s \gg T_{\text{CBR}}$ so that $\delta T_b \propto x_{\text{HI}}(1+\delta^s)$ up to a multiplicative constant. We further substitute the expansion (2) for x_{HI} and write $x_{\text{HI}}(1+\delta^s) \propto \mathcal{M}(\mathbf{r})[1+(b-1)\delta^r + \delta^s]$ to first order in δ , where $b = 1 + \partial \ln x_{\text{HI}}/\partial \delta$ (see also Barkana & Loeb 2004). Note that x_{HI} is determined by the real space

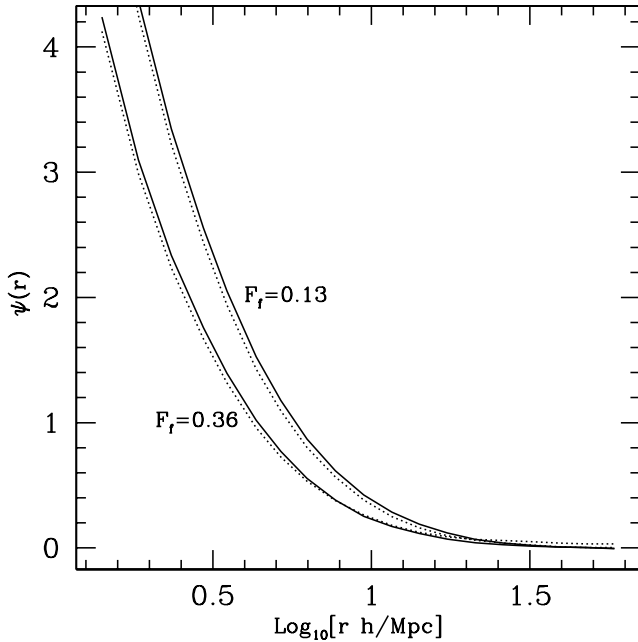


Figure 3. The correlation ψ as a function of separation, for two values of the filling factor of ionized regions, as indicated in the figure. The upper ($F_{\text{fill}} = 0.13$) and lower sets ($F_{\text{fill}} = 0.36$) of curves are for sources identified as 4σ and 3.5σ peaks in the density field, respectively. The solid lines show the correlation when the mask of ionized regions is placed around the peaks, while the dotted lines are for masks displaced away from the peaks.

density δ^r , hence the appearance of δ^r . For simplicity we will assume that the data yields the quantity

$$d(\mathbf{r}) = \mathcal{M}(\mathbf{r})\Delta^s, \quad (18)$$

where $\Delta^s = 1 + (b-1)\delta^r + \delta^s$. Using the linear relation (5) we find that $\Delta^s = (b-1)\delta^r + \delta^s = b\delta^r - dU/dr$ which can be identified as the redshift space density contrast corresponding to the real space density field $\Delta^r = b\delta^r$.

We write the data-data redshift space correlation function as

$$\psi^s = \langle dd \rangle = \xi_{\mathcal{M}}(r)[1 + \xi^s(\mathbf{r})], \quad (19)$$

where $\xi_{\mathcal{M}} = \langle \mathcal{M}\mathcal{M} \rangle$ is the correlation function of the mask, and ξ^s is now the correlation function of Δ^s . We have also assumed that the mask x_{HI} and δ are uncorrelated (but see Furlanetto, Zaldarriaga & Hernquist 2004, Zaldarriaga, Furlanetto & Hernquist 2004). This assumption is justified once the filling factor of ionized regions is larger than $\bar{n}R_c^3$ where \bar{n} is the number density of sources and R_c is the coherence length of the correlations between the sources and the gas. This condition is easily satisfied as a single source is capable of ionizing relatively large regions around it. To test this assumption we have resort to our random gaussian density field having a Λ CDM power spectrum (see figure 2). We identify the sources as peaks in the density smoothed with $1 \text{ h}^{-1}\text{Mpc}$ and assume that each source ionizes a region of a given radius around it. These regions define a mask which we then displace randomly through the box. A comparison between the correlation of the mask times the density field when the mask is placed around the sources and

when it is placed randomly in the box serves as an indication to the the degree of correlation between the mask and the density field. In figure (3) the solid lines are the correlation function ψ (in real space) for a mask placed around the sources while the dotted are the correlations when the mask is placed randomly in the box. The upper and lower sets of curves correspond to two values of the filling factor, F_{fill} , of ionized regions. The values $F_{\text{fill}} = 0.13$ and 0.36 , respectively, correspond to sources identified as 4σ and 3.5σ peaks. The differences between the dotted and solid curves for each value of the F_{fill} are negligible.

We will write now the expressions describing the anisotropy of the data-data correlation function in the presence of geometrical and redshift distortions. We restrict the analysis to the linear regime $\delta \ll 1$ and to first order in α .

We write $\tilde{\xi}^s(\tilde{r}_{\parallel}, \tilde{\mathbf{r}}_{\perp}) = \xi^s((1 + \alpha)\tilde{r}_{\parallel}, \tilde{\mathbf{r}}_{\perp})$ and use (7) to express ξ^s in terms of the moments $\xi_l(r)$ with $(r = \sqrt{(1 + \alpha)^2\tilde{r}_{\parallel}^2 + \tilde{\mathbf{r}}_{\perp}^2})$ and Legendre polynomials evaluated at $\mu = (1 + \alpha)\tilde{r}_{\parallel}/\tilde{r}$. Then we use (16) and (17) to expand ξ_l and P_l as functions of \tilde{r} and $\tilde{\mu}$ to first order in α . The final result of this straightforward algebra is

$$\begin{aligned} \tilde{\psi}^s(\tilde{r}_{\parallel}, \tilde{\mathbf{r}}_{\perp}) &= \sum_{l=0,2,4} \psi_l(\tilde{r}) P_l(\tilde{\mu}) \\ &+ \alpha \sum_{l=0,2,4} \psi_l(\tilde{r}) \left[\frac{d \ln \psi_l(\tilde{r})}{d \ln \tilde{r}} \tilde{\mu}^2 P_l(\tilde{\mu}) + \tilde{\mu}(1 - \tilde{\mu}^2) \frac{d P_l(\tilde{\mu})}{d \tilde{\mu}} \right] \\ &= \sum_{l=0,2,4} [\psi_l(\tilde{r}) + \alpha a_l(\tilde{r})] P_l(\tilde{\mu}) + \alpha a_6(\tilde{r}) P_6(\tilde{\mu}) \end{aligned} \quad (20)$$

where $\psi_0 = \xi_{\mathcal{M}}(1 + \xi_0)$ and $\psi_l = \xi_{\mathcal{M}}\xi_l$ for $l > 0$, and

$$\begin{aligned} a_0 &= \frac{1}{3} \psi_0 \frac{d \ln \psi_0}{d \ln \tilde{r}} + \psi_2 \left(\frac{2}{5} + \frac{2}{15} \frac{d \ln \psi_2}{d \ln \tilde{r}} \right) \\ a_2 &= \frac{2}{3} \psi_0 \frac{d \ln \psi_0}{d \ln \tilde{r}} + \psi_2 \left(\frac{2}{9} + \frac{11}{21} \frac{d \ln \psi_2}{d \ln \tilde{r}} \right) \\ &+ \psi_4 \left(\frac{20}{21} + \frac{4}{21} \frac{d \ln \psi_4}{d \ln \tilde{r}} \right) \\ a_4 &= -\psi_2 \left(\frac{24}{35} - \frac{12}{35} \frac{d \ln \psi_2}{d \ln \tilde{r}} \right) + \psi_4 \left(\frac{20}{77} + \frac{39}{77} \frac{d \ln \psi_4}{d \ln \tilde{r}} \right) \\ a_6 &= -\psi_4 \left(\frac{40}{33} - \frac{10}{33} \frac{d \ln \psi_4}{d \ln \tilde{r}} \right). \end{aligned} \quad (21)$$

The visual impression between geometrical and redshift distortions seen in figure (2) is quantified by the relation (20). The moments a_l and ψ_l , respectively, characterize the geometrical and redshift distortions. A term containing P_6 is missing from the redshift distortions of the correlations. One could determine the correct value of the distance ratio, α , by minimizing the P_6 term in the correlation function. Nevertheless, we describe below other ways as well. Let us inspect the moments a_l and ψ_l . The moments depend on the linear correlation function. Here we use the linear correlation obtain from the power spectrum of the Λ CDM model with $\Omega_m = 0.3$. Figure (4) shows the ratio of the moments a_l/ψ_l for $l = 0, 2$, and 4 . Also shown is a_6 multiplied by a factor of 10 for the sake of clarity. In computing the moments we have assumed that the mask correlation function, $\xi_{\mathcal{M}}$, is unity. The mask correlation function affects only the

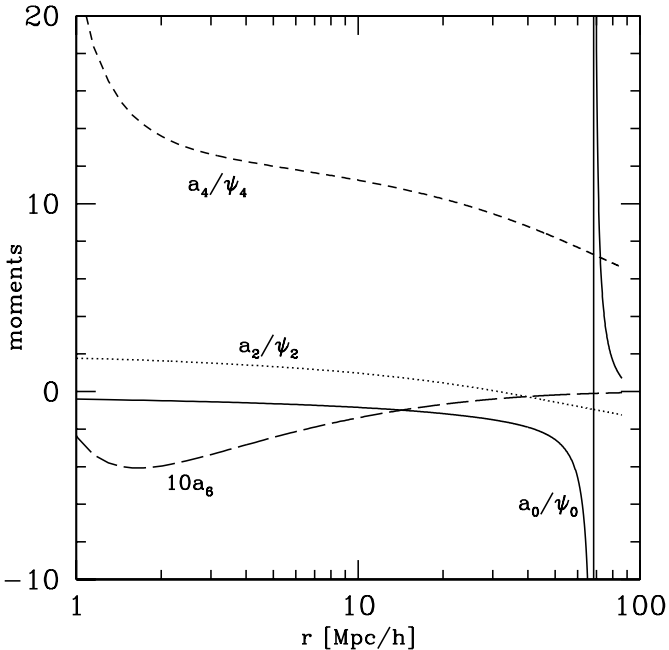


Figure 4. Ratios of the moments, a_l/ψ_l ($l = 0, 2, 4$), as a function of separation. Also shown is the moment a_6 multiplied by a factor of 10. All curves correspond to the linear correlation function of Λ CDM with $\Omega_m = 0.3$, assuming that the correlation of the mask is unity.

terms containing ψ_0 and so a_4/ψ_4 and a_6 are not affected by this correlation anyways. The ratio $|a_0/\psi^0|$ is small except at separations of $r \sim 60 \text{ h}^{-1}\text{Mpc}$ where measuring the correlations is probably hard. The moments a_2 and a_4 are larger than ψ_2 and ψ_4 by a factor of 2 and 10, respectively, making the anisotropy pattern a very sensitive function of α . A comparison between the moments $\int \psi^s(\tilde{\mu}) P_l(\tilde{\mu}) d\tilde{\mu}$ should provide significant constraints on α , the bias parameter β , and possibly on the form of the mask.

6 DISCUSSION

We have discussed the application of the Alcock-Paczynski test to maps of the redshifted 21-cm emission from the era of reionization. Our two main conclusions are a) at $z \sim 20$ the ratio of the frequency to angular distance scales is sensitive to the assumed cosmological parameters and the equation of state of the dark energy, and b) that geometrical distortions resulting from an erroneous choice for the cosmological parameters are very distinct from redshift distortions caused by peculiar motions. Judging by the ratio of the moments (see figure 4) A determination of the correlation of temperature fluctuations to an accuracy of 20% should allow a successful application of the AP test. The prospects for measuring the cosmological 21-cm signal are good in view of the planned telescopes like the Low Frequency Array [‡] (LOFAR),

[‡] <http://www.lofar.org>

the Primeval Structure Telescope [§] (PAST), and the Square Kilometer Array [¶]. It remains to be seen how well the correlation function will be determined from data provided by these telescopes. The application of the AP test to 21-cm maps can be hindered by contaminations from bright foreground sources (e.g. Oh & Mack 2003; Di Matteo et al. 2002; Di Matteo, Ciardi & Muniati 2004). However, removal of this contamination should be possible by a proper identification of the sources.

7 ACKNOWLEDGMENT

This work is supported by the Research and Training Network “The physics of the Intergalactic Medium” set up by the European Community under the contract HPRNCT-2000-00126 and by the German Israeli Foundation for the Development of Research. The author is grateful to the Institute for Advanced Study (Princeton) and the Institute of Astronomy (Cambridge) for the hospitality and support.

REFERENCES

Alcock C., Paczyński B., 1979, Nature, 281, 358
 Bahcall N.A., et al., 2003, ApJ, 585, 182
 Baltz E.A., Gnedin N.Y., Silk, J., 1998, ApJ, 493, 1
 Barkana R., Loeb A., 2004, astro-ph/0409572
 Barreiro T., Bento M.C., Santos N.M., Sen A.A., 2003, Phys.Rev D, 68, 3515
 Benson A.J., A., Sugiyama N., Lacey C., 2001, MNRAS, 320, 153
 Bruscoli M., Ferrara A., Fabbri R., Ciardi B., 2000, MNRAS, 318, 1068
 Caldwell R.R., Doran M., 2004, Phys.Rev D., 69, 3517
 Caresias P., Matarrese S., Moscardini L., 2004, ApJ, 605, 21
 Coble K., Dodelson S., Frieman J.A., Phys.Rev D, 55, 1851
 Chen X., Miralda-Escude J., 2004, ApJ, 602, 1
 Ciardi B., Madau P., 2003, ApJ, 596, 1
 Cole A., Fisher K.B., Weinberg D.H., 1994, MNRAS, 267, 785
 Croft R.A.C., Weinberg D.H., Bolt M., Burles S., Hernquist L., Katz N., Kirkman D., Tytler D., 2002, ApJ, 581, 20
 Davis M., Peebles P.J.E., 1983, ApJ, 267, 465
 Desjacques V., Nusser A., Haehnelt M.G., Stoehr F., 2004, MNRAS, 350, 879
 Di Matteo T., Ciardi B., Muniati F., 2004, astro-ph/0402322
 Di Matteo T., Perna R., Abel T., Rees M.J., 2002, ApJ, 564, 576
 Field G.B., 1958, Proc. IRE, 46, 240
 Field G.B., 1959, ApJ, 129, 551
 Fisher K.B., Nusser A., 1996, MNRAS, 279, 1
 Furlanetto S.R., Sokasian A., Hernquist L., 2004, MNRAS, 347, 187
 Furlanetto S.R., Zaldarriaga M., Hernquist L., 2004, ApJ, 613, 16
 Gnedin N.Y., Shaver P.A., 2004, ApJ, 608, 611
 Hamilton A.J.S., 1992, ApJ, 385, 5
 Hatton S., Cole S., 1998, MNRAS, 296, 10
 Hogan C.J., Rees M.J., 1979, MNRAS, 188, 791
 Hui L., Stebbins A., Burles S., 1999, ApJ, 511, 5
 Ikebe Y., Reiprich T.H., Böhringer H., Tanaka Y., Kitayama T., 2002 A&A, 383, 773

[§] <http://astrophysics.phys.cmu.edu/jbp>

[¶] <http://www.skatelescope.org>

Kaiser N., 1987, MNRAS, 227, 1

Knop R., et al. , 2003, ApJ, 598, 102

Knox L., Scoccimarro, R., Dodelson S., 1998, Phys.Rev D, 81, 2004

Kunz ., Corasaniti P.S., Parkinson D., Copeland E.J., 2004, Phys.Rev D, 70, 1301

Lima J.A.S., Alcaniz J.S., 2000, A&A, 357, 393

Madau P., Meiksin A., Rees M.J., 1997, ApJ, 475, 429

McDonald P., Miralda-Escudé J., Rauch M., Sargent W.L.W., Barlow T.A., Cen R., Ostriker J.P., 2000, ApJ, 543, 1

McDonald P., Seljak U., Cen R., Weinberg D.H., Burles S., Schneider D.P., Schlegel D.J., Bahcall N.A., Briggs J.W., Brinkmann J., Fukugita M., Ivezić Z., Kent S., Vanden Berk D.E., 2004, astro-ph/0407377

Nusser A., Haehnelt M., 2000, MNRAS, 313, 364

Nusser A., Davis M., 1994, ApJ, 421

Nusser A., Davis M., Willick J.A., 1996, ApJ, 473

Nusser A., 2004, astro-ph/0409640

Oh S.P., Mack K.J., 2003, MNRAS, 346, 871

Peebles P.J.E., *The Large Scale Structure in the Universe*, Princeton Univ. Press.Princeton, NJ

Peacock J.A., 1999, *Cosmological Physics*, Cambridge Univ. Press. Cambridge

Percival W.J., et al. , 2002, MNRAS, 337, 1068

Ratra B., Peebles P.J.E., 1988, Phys.Rev D, 37, 3406

Ricotti M., Ostriker J., 2004, MNRAS,352, 547

Ricotti M., Ostriker J., Gnedin N.Y.,2004, astro-ph/0404318

Riess A., et al. , 2004, ApJ, 607, 665

Scott D., Rees M.J., 1990, MNRAS, 247, 510

Spergel D.N. et al. , 2003, ApJS, 148, 175

Strauss M.A., Willick J.A., 1995, Phys.Rep., 261, 271

Sunyaev R.A., Zel'dovich Y.A., 1975, MNRAS, 171,375

Subramanian K., Padmanabhan T., 1993, MNRAS, 265, 101

Taylor A.N., Hamilton A.J.S., 1996, MNRAS, 282, 767

Tegmark M., et al. 2004, ApJ, 606, 702

Turner M.S., White M.J., Phys.Rev. D, Lett. 80, 1582

Tozzi P., Madau P., Meiksin A., Rees M.J., 2000, ApJ, 528, 597

Vauclair S.C., Blanchard A., Sadat R., Bartlett J.G., Bernard J.P., Boer M., Giard M., Lumb D.H., Marty P., Nevalainen J., 2003, A&A, 412, 37

Viel M., Weller J., Haehnelt M., 2004, astro-ph/0407294

Wetterich C., 1995, A&A, 301, 321

Wild J.P., 1952, ApJ, 115, 206

Zaldarriaga M., Furnaletto S.R., Hernquist L., 2004, ApJ, 608, 622

Zaroubi S., Hoffman Y., 1996, ApJ, 462, 25

Zaroubi S., Bernardi M., da Costa L.N., Hoffman Y., Alonso M.V., Wegner G., Willmer C.N.A., Pellegrini P.S., 2001, MNRAS, 326, 375

Zehavi E., et al. , 2002, ApJ, 571, 172